Spin-glass shell and magnetotransport properties of a $La_{0.67}Ca_{0.33}MnO_3$ nanoring network

M. H. Zhu,[1] Y. G. Zhao,[1,*] W. Cai,[1] X. S. Wu,[2] S. N. Gao,[1] K. Wang,[1] L. B. Luo,[1] H. S. Huang,[1] and L. Lu[2]
[1]*Department of Physics, Tsinghua University, Beijing 100084, People's Republic of China*
[2]*Institute of Physics, Chinese Academy of Sciences, Beijing 100080, People's Republic of China*
(Received 11 June 2006; revised manuscript received 12 December 2006; published 27 April 2007)

The magnetotransport and magnetic property of the $La_{0.67}Ca_{0.33}MnO_3$ (LCMO) nanoring network (NRN) have been investigated. This NRN-LCMO shows a giant magnetoconductance at low temperatures with strong memory effect of magnetic field. Its high field magnetoconductance shows linear field dependence with an anomalously abrupt increase of slope at about 4 T. The magnetic field dependence of the resistance peak in the resistance vs temperature curve strongly depends on the grain size. The most interesting results are the exchange bias effect of magnetization and the resistance relaxation at low temperatures, which suggest the existence of two types of spin glass in the shell of LCMO grains. The magnetotransport behavior of NRN-LCMO was explained by considering the role of the spin-glass shell in the tunneling process with a core-shell model. We emphasized that the shell layers are magnetized by both the external magnetic field and the internal magnetic field induced by the ferromagnetic cores. This work also indicates that the electronic transport of NRN-LCMO can provide some important information on the magnetic state of the nanograin shell.

DOI: 10.1103/PhysRevB.75.134424 PACS number(s): 75.47.Gk, 73.50.−h, 75.75.+a

I. INTRODUCTION

The effect of grain boundary on the magnetoresistance (MR) of manganites with colossal magnetoresistance (CMR), is an important topic and has been extensively studied because of its rich physics as well as the potential applications.[1–26] Hwang *et al.* observed a striking MR response in polycrystalline $La_{0.67}Sr_{0.33}MnO_3$, i.e., an abrupt resistance drop in low fields (LFMR) followed by a slow decrease in high field (HFMR), which demonstrates the importance of grain boundary in determining the MR of polycrystalline samples.[1] Polycrystalline manganites with ultrafine grains,[13,16–26] in their own right, are attractive because their electronic transport is dominated by the grain boundary. In fact, the grain boundary region increases with the decreasing grain size, making the grain boundary more important in determining the electronic transport property of manganites with ultrafine grains.

So far, the samples used in the study of CMR manganites with ultrafine grains were obtained by the low-temperature sintering or mechanical alloying.[13,16,18–26] In our previous papers,[14,15] an approach was used to get nano-CMR $La_{0.67}Ca_{0.33}MnO_3$ (LCMO) samples by using the pulsed laser deposition of LCMO on porous Al_2O_3. The samples showed a nanoring network (NRN) of LCMO with the nanograins being connected in one or two dimensions, which is quite different from the three-dimensional connection in the bulk samples with ultrafine grains.[13,16,18–26] We found that the T_p of NRN-LCMO decreases with the decreasing average thickness of the films and their temperature dependence of the coercive field (H_c) follows $H_c(T)=H_c(0)[1-(T/T_B)^{1/2}]$, a relation that has been well established in nanoferromagnetic metals and alloys in the superparamagnetic regime below the blocking temperature T_B. Furthermore, the resistance and magnetization data of NRN-LCMO at zero field cooling (ZFC) and field cooling (FC) suggest the possible existence of two types of spin glass in the grain boundary region. Considering the important role of grain boundary in determining the electronic transport of nano-CMR manganites, it is essential to get further evidence from more direct experiments, such as the magnetic measurement. There are other issues in the nano-CMR manganites that need to be clarified. For example, it has been shown that the temperature dependence of resistance for manganites with nanograins showed a resistance peak at a certain temperature (T_p), remarkably lower than the Curie temperature (T_C) of the samples,[19,21–24] in contrast to the consistence of T_p and T_C in the single crystals, polycrystalline bulk samples, and the epitaxial thin films of CMR. The origin of the difference between T_p and T_C and the nature of this resistance peak is still an open question despite the vast amount of work.

In this paper, we focus on the characterization of the magnetic property of the grain boundary and the magnetotransport property of the NRN-LCMO in order to get some insight into the magnetic state of the grain boundary and the mechanism of the electronic transport in NRN-LCMO and the role of magnetic field. The following interesting results were obtained. (1) Exchange bias effect of magnetization and the resistance relaxation under zero external magnetic field were observed. These results strongly support the existence of two types of spin glass in the grain boundary. (2) NRN-LCMO shows giant magnetoconductance (MC), which is much larger than those of the nano-CMR manganites with ultrafine grains obtained by other approaches. Moreover, the MC of NRN-LCMO exhibits two linear HFMC regions with an anomalous increase of slope at about 4 T, in contrast to the one linear HFMC region in $La_{0.7}Sr_{0.3}MnO_3$ nanopolycrystalline samples up to 47 T as reported in Ref. 4. (3) The effect of the external magnetic field on the temperature-dependence of resistance was carefully studied and it was found that T_p shows a remarkable increase with magnetic field for samples with small grain sizes (thinner films). Surprisingly, T_p for the thicker films shows unusual insensitivity to the magnetic field even though the magnetic field is very strong. In order to understand the properties of NRN-LCMO, we proposed a unified picture by considering the multistep

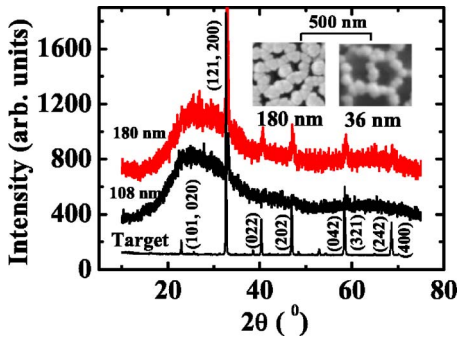

FIG. 1. (Color online) X-ray-diffraction pattern of the NRN-LCMO and the LCMO target. The insets are their SEM morphology.

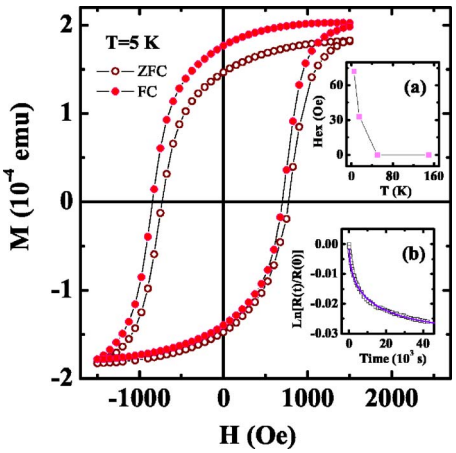

FIG. 2. (Color online) Hysteresis loops of the 108-nm NRN-LCMO sample at $T=5$ K with $H_{cool}=1500$ Oe for FC process. Inset (a): exchange bias H_{ex} vs temperature. Inset (b): resistance relaxation recorded at 80 K under zero external magnetic field.

inelastic tunneling through the grain boundary in the frame of core-shell model. It is emphasized that the shell layers of the grains are magnetized by both the external magnetic field and the internal magnetic field induced by the ferromagnetic cores, and the magnetization of the shell layers plays a key role in the magnetic tunneling process between nanograins. The unique configuration of NRN-LCMO provides a way to get some insight into the role of the grain boundary in the electronic transport of the manganites with nanograins.

II. EXPERIMENTAL

NRN-LCMO thin films were obtained by growing LCMO on porous Al_2O_3 arrays with holes of 200 nm average diameter. The fabrication process of NRN-LCMO was described in detail in our previous paper.[15] The average thickness of the sample was obtained by calibration on film grown on crystalline $LaAlO_3$. A LCMO film was deposited on $LaAlO_3$ substrate with the same process as NRN-LCMO thin films and its deposition rate was used to get the nominal thickness of NRN-LCMO sample.

Phase analysis of the samples was performed using a Rigaku D/max-RB x-ray diffractometer with CuK_α radiation. The surface morphology of the LCMO films was investigated by using field emission scanning electron microscopy (FESEM-LEO1530).

The resistance of the samples was measured by the standard four-probe method. Silver paste was used for the electrical contacts. The magnetic properties were performed in a Quantum Design Magnetic Property Measurement System (MPMS-XL7). The low-temperature and high-field conditions of a Quantum Design Physical Property Measurement System (PPMS) was used to study the effect of magnetic field on the electrical transport property of NRN-LCMO with the magnetic field parallel to the sample surface.

III. RESULTS AND DISCUSSION

Figure 1 shows x-ray-diffraction patterns of the NRN-LCMO samples and the LCMO target, indicating that the phase of NRN-LCMO is similar to that of the LCMO target. Thus it can be inferred that the NRN-LCMO is a single phased polycrystalline sample. The x-ray diffraction pattern for the 36 nm sample is not available because of its much thinner thickness and the resultant weak signal. The SEM images of NRN-LCMO are shown in the inset of Fig. 1. A LCMO nanoring network was obtained for a 36-nm-thick film. With increasing average film thickness via increasing deposition time, the grain size of LCMO increases and the nanorings of LCMO were replaced by compact packaging of larger grains.

In order to get some insight into the magnetic state of the grain boundary, we measured the magnetization of NRN-LCMO with FC and ZFC. Figure 2 presents the FC and ZFC hysteresis loops of 108-nm NRN-LCMO at 5 K. The sample was cooled down to the measuring temperature under a cooling field $H_{cool}=1500$ Oe for FC and $H_{cool}=0$ Oe for ZFC, and the hysteresis loop measurement started. The FC hysteresis loop has an obvious shift towards the negative H values compared to its ZFC counterpart. This shift of FC loop from its ZFC loop is called "exchange bias" effect and quantified through the exchange field parameter $H_{ex}=|H_{right}+H_{left}|/2$, H_{right} and H_{left} being the points where the loop intersects $M=0$ axis. The exchange bias effect has often been observed in samples with a ferrimagnet or ferromagnet (FM) surrounded by a layer of antiferromagnet (AFM) (FM/AFM) in the case of AFM Néel temperature $T_N<T_c$, as well as in samples involving a spin-glass (SG) phase (FM/SG) when frozen temperature $T_g<T_c$.[27–30] The origin of the exchange bias effect is the exchange coupling at the interface of FM/AFM or FM/SG so as to minimize the interface exchange energy. For a FM/SG system, while the sample is cooled through T_g in an external magnetic field (FC process), exchange coupling at the interface of magnetized FM and SG leads to a preferred FM spin orientation and SG configuration, and an exchange anisotropy appears. As a result, when a FM/SG system is cooled through T_g with the FC process, the exchange anisotropy will manifest itself in the form of a shift of the hysteresis loop towards negative H values (exchange bias H_{ex}). Because the inner part of the grain in our NRN-LCMO films is FM, the appearance of the exchange bias effect in the NRN-LCMO film indicates that either the

SG or AFM phase at the grain boundary of the film is adjacent to the FM inner part of the grain.

To further probe the magnetic state at the grain boundary of NRN-LCMO, the experiment on resistance relaxation under zero external magnetic field is necessary. If a SG exists at the grain boundary, the SG will be slowly aligned by the FM inner part of the grain below T_g, leading to a gradual decrease of tunneling barriers and subsequent resistance drop. Therefore, the resistance relaxation phenomenon is expected even though the external magnetic field is zero. For this purpose, the 108-nm NRN-LCMO sample is cooled to 80 K at 6 K/min without external magnetic field. After the temperature is stable at 80 K, the change of resistance with time was recorded and the result is shown in the inset (b) of Fig. 2. The observation of relaxation phenomenon excludes AFM phases. The relaxation data are well fitted by the stretched exponential function $\ln[R(t)/R(0)]/\ln[R(\infty)/R(0)] = 1-\exp[-(t/\tau)^{\beta}]$, where $R(0)$ and $R(\infty)$ denote the resistance of the sample at $t=0$ s and the equilibrium state, respectively, τ represents the characteristic relaxation time and is described by the equation $\tau=A\exp(\Delta/k_BT)$ with Δ and k_B being the thermal activation energy and the Boltzmann constant, respectively. The fitting of the result gives $\tau=12501$ s, $\beta=0.5$ as shown by the solid line in the figure. The deviation of β from 1 is related to the multiple relaxation processes, implying a wide distribution of the potential barriers.[31,32]

The resistance relaxation and the exchange bias effect discussed above indicate the existence of spin glass at the grain boundary. The inset (a) of Fig. 2 illustrates the temperature dependence of the exchange bias H_{ex} obtained from its FC hysteresis loops with the same cooling field 1500 Oe. H_{ex} at 15 K reduces to 32 from 72 Oe at 5 K and becomes zero at 50 and 150 K. As the H_{ex} is determined by the frozen configuration of the spin glass through the exchange coupling at the FM/SG interface, the H_{ex} data indicate that T_g for the spin glass at the grain boundary is below 50 K. This type of spin glass is adjacent to the inner FM part of NRN-LCMO grain and called the type I spin glass. The relaxation behavior at 80 K suggests that another type of spin glass also exists at the grain boundary with its frozen temperature larger than 80 K. Such a type of spin glass is separated from the FM inner part by the type I spin glass and is called type II spin glass since H_{ex} becomes zero at the temperature larger than 50 K. Hence, the combination of the exchange bias effect and the resistance relaxation behavior gives a strong support to the existence of two types of spin glass in the grain boundary.

Figure 3 shows the magnetic field dependence of the resistance for a 36-nm-thick NRN-LCMO sample at 10 K with increasing and decreasing magnetic field. In this measurement, the magnetic field was increased to 14 T at a fixed rate of 100 Oe s^{-1} and stayed for 2 h at 14 T, and then decreased at the same rate. The inset is the magnetic field dependence of the resistance for 180 nm NRN-LCMO at 10 K, which was measured in the same way as 36-nm-thick NRN-LCMO sample. Surprisingly, the resistance of the sample doesn't recover with decreasing field, showing a big hysteresis for 36-nm-thick film. The *R-H* curves of 180-nm film show much smaller hysteresis than that of 36-nm film. So the thinner NRN-LCMO film has a stronger magnetic memory effect. The increasing field curves of Fig. 3 show that both samples own the typical LFMR behavior with a sharp drop of resistance below about 0.5 T and HFMR behavior with a slow resistance decrease above 0.5 T. Lee *et al.*[8] proposed an inelastic tunneling model to account for the LFMR and HFMR phenomena, giving a good explanation for the observed LFMR upper limit of 30–40 %. And by considering higher order inelastic tunneling processes, Ziese *et al.*[3] explained the temperature dependence of the LFMC. The inelastic tunneling model predicts a linear high magnetic field dependence of magnetoconductance (HFMC) instead of HFMR, i.e., HFMC is proportional to the susceptibility of the grain boundary and the external magnetic field. The magnetoconductance MC is defined by $MC=[G(H)-G(0)]/G(0)$, where $G(H)$ and $G(0)$ correspond to the conductivity in an applied field H and zero applied field, respectively. The magnetic field dependence of MC for the NRN-LCMO samples was calculated from their increasing field *R-H* data and is depicted in Fig. 4. MC-*H* curve from 0 to 1.2 T is shown as inset of Fig. 4 to show the transition from LFMC (less than 0.5 T) to HFMC. The HFMC shows the linear dependence on magnetic field with an anomalously abrupt increase of slope at about 4 T, i.e., two linear HFMC regions, in contrast to the one linear HFMC region reported in the literature.[4,8,13,19] The existence of the two linear HFMC regions implies that the grain boundary's susceptibility is not constant as discussed later. In addition, the MC of 36-nm

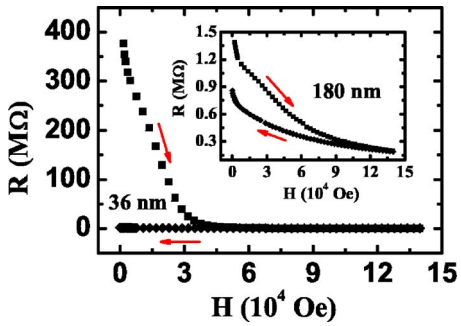

FIG. 3. (Color online) Magnetic field dependence of the resistance for a 36-nm-thick NRN-LCMO film at 10 K with increasing and decreasing magnetic field. The inset is the magnetic field dependence of the resistance for a 180-nm-thick NRN-LCMO film at 10 K with increasing and decreasing magnetic field.

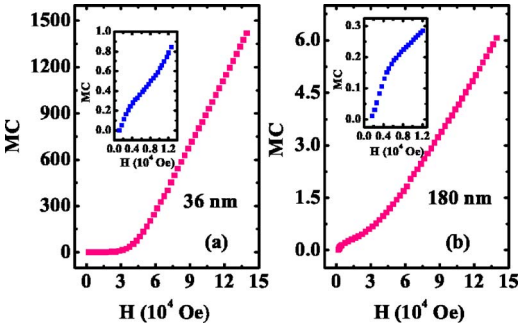

FIG. 4. (Color online) Magnetoconductance as a function of increasing magnetic field. (a) 36-nm sample, (b) 180-nm sample. The inset is an expand view of low magnetic field region.

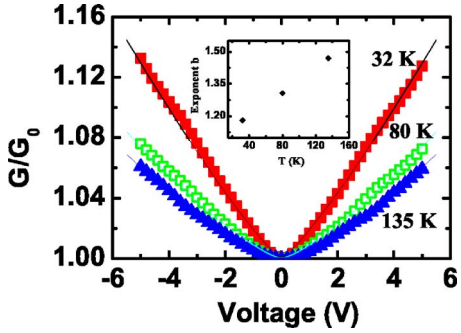

FIG. 5. (Color online) Dynamic conductance $G=dI/dV$ as a function of applied voltage for 36-nm NRN-LCMO sample under zero magnetic field. The solid lines are fits of Eq. (1) to the data. The fitting result of the dynamic conductance exponent b is shown in the inset.

NRN-LCMO is 525 at 8 T and 10 K, which is remarkably larger than the MC value of 3 in bulk LCMO samples with ultrafine grains under similar conditions.[22] This demonstrates the advantage of our NRN preparation technique, which can increase MC in CMR materials dramatically.

In order to further recognize the multistep inelastic tunneling process of the electronic transport across grain boundaries in the NRN-LCMO samples. The current-voltage (I-V) curves were measured under zero magnetic field for the 36-nm NRN-LCMO sample at 32, 80, and 135 K, respectively. The dynamic conductance, defined as $G=dI/dV$, was calculated from the I-V curves and the result is shown in Fig. 5 with G_0 denoting the conductance in the zero voltage limit. We fitted G/G_0 with the following expression to describe the tunneling I-V feature with a and b being measure of the weight of the nonlinear transport:

$$G/G_0 = 1 + aV^b. \quad (1)$$

In the case of direct elastic tunneling through the grain boundary barrier, the exponent b equals 2 at low voltages, which is described by the quantum tunneling theory of Simmons.[33] If the transport is dominated by the inelastic tunneling via localized states at grain boundaries, Glazman and Matveev (GM) predict that b is nonquadratic.[34] The fitted exponent b depicted in the inset of Fig. 5 ranges from 1.2 to 1.5, indicating that the inelastic tunneling via localized states is the dominant transport mechanism below T_c in the NRN-LCMO. The number of inelastic channels and the fraction of charge carriers entering each inelastic channel change with temperatures. At higher temperatures, more inelastic channels are available, leading to the increase of exponent b.[3,5]

Shown in Fig. 6 is the effect of magnetic field on the temperature dependence of the resistance for NRN-LCMO with different thicknesses. It can be seen that resistance peak T_p is well below the paramagnetic-ferromagnetic (PM-FM) transition temperature T_c, which was measured to be about 250 K in all the NRN-LCMO samples.[15] Its T_c value indicates that the inner parts of the grains are similar to the $La_{0.67}Ca_{0.33}MnO_3$ bulk or thin film samples with metallic conductivity and FM below T_c. In addition, it is noted that

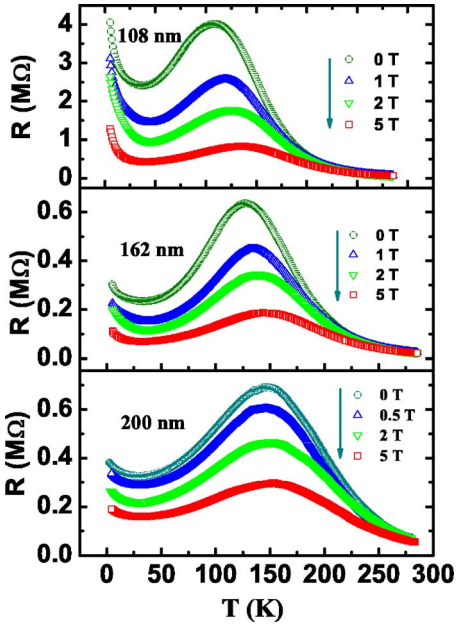

FIG. 6. (Color online) Effect of magnetic field on the temperature dependence of the resistance for NRN-LCMO with different thicknesses.

the electrical resistance peak of the thinner films shifts to high temperatures upon applying magnetic field, in contrast to that of the thicker film which does not show an obvious shift to high temperatures although its peak resistance drops remarkably. The magnetic field dependence of T_p for the NRN-LCMO with different thicknesses was shown in Fig. 7. The insensitivity of T_p to magnetic field for the thicker film is very unusual. Chen *et al.* reported the growth of (001)/(110) mixed aligned $La_{2/3}MnO_3$ film on Al_2O_3 single crystal and found that the T_p of this film is remarkably lower (195 K) than T_c and remains unchanged even if 5 T magnetic field was applied, in contrast to the films grown on $SrTiO_3$.[10] They believed that the anomaly was related to the grain boundaries. In our present work, the dependence of T_p on sample thickness and magnetic field is investigated systematically. T_p of the thinner film shows magnetic field dependence while T_p of the thicker film is insensitive to magnetic field. This thickness dependence of T_p is helpful for understanding the nature of the resistance peak.

To discuss the results shown in Figs. 3, 4, and 6 within a unified picture, we need to consider the transport of electrons

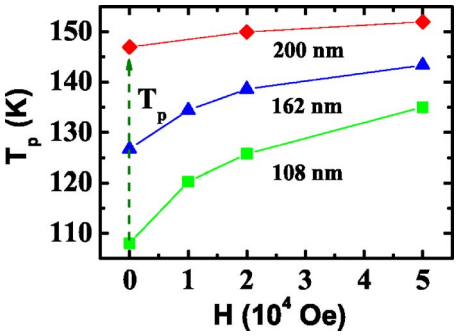

FIG. 7. (Color online) Variation of T_p with magnetic field for NRN-LCMO with different thicknesses.

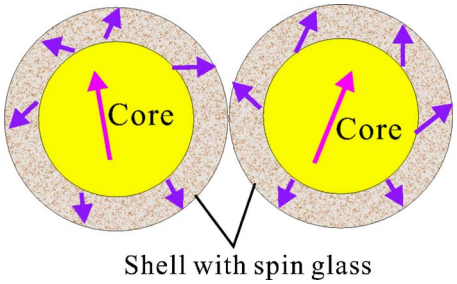

FIG. 8. (Color online) The connection of two grains with core and shell.

from one grain to another. As proposed in our previous paper in terms of core-shell model[14] and demonstrated in the present paper, each grain contains core and shell. The connection of two grains with core and shell is illustrated in Fig. 8. The core is the inner part of the grain, being metallic and ferromagnetic (FM) below T_c. Because the grain size is very small (see Ref. 14, about 60 nm for 180-nm-thick film), it is expected that one grain contains a single magnetic domain below T_c, called a FM core. The shell layer, being located on the surface of the grain and extending into the grain with a certain depth, is magnetically disrupted and contains two types of spin glass with different T_g as established above. The adjacent shells of the grains constitute the grain boundary of the polycrystalline NRN-LCMO. With the reduction of the average thickness of the NRN-LCMO films, the grain size decreases and thus the thickness of the magnetically disordered shell layer increases as shown by Balcells.[20] Moreover, the connectivity between the grains also weakens with decreasing grain size.

Because the core of the grains is FM and metallic below T_c, the resistance of the NRN-LCMO mainly originates from the grain boundary tunneling barrier. Thus the transport property of the NRN-LCMO is determined mainly by the grain boundary tunneling resistance (R_b). R_b is expected to be proportional to $\exp[(E_c+E_m)/2k_BT]$:[35,36]

$$R_b \propto \exp\frac{E_c + E_m}{2k_BT}, \tag{2}$$

where E_c is the charging energy of the nanograins, E_m is the magnetic tunneling barrier of grain boundary, and k_B is the Boltzmann constant. The $\exp(E_m)/2k_BT$ term was introduced by Helman and Abeles[35] in order to account for MR in granular magnetic metals, and E_m is the magnetic barrier energy associated with the spin orientation of the two neighboring grains and can be expressed as

$$E_m = \frac{1}{2}J[1 - \langle \vec{S}_1 \bullet \vec{S}_2 \rangle / S^2], \tag{3}$$

where J is the exchange coupling constant within inner parts of the grains and $\vec{S}_1, \vec{S}_2$ are the spins of the two neighboring grains with the same magnitude S. In the NRN-LCMO, the MC-H and I-V characteristics favor the multistep inelastic tunneling model,[3] and Eq. (3) can be reasonably written as

$$E_m = \frac{1}{2}J[1 - \langle \hat{s}_1 \cdot \hat{s}_{b1} \rangle \langle \hat{s}_{b1} \cdot \hat{s}_{b2} \rangle \cdots \langle \hat{s}_{bn} \cdot \hat{s}_2 \rangle], \tag{4}$$

where $\hat{s}_{bn}$ is the unit vector along the direction of Mn spin of n sites in the shell layer corresponding to the nth order inelastic channel, and $\hat{s}_1, \hat{s}_2$ are the unit vectors along the direction of Mn spins of two neighboring cores, respectively. Equation (4) implies that the magnetic tunneling barrier in the multistep inelastic tunneling process is strongly associated with the spin alignment in the shells and the magnetic moment orientation of the adjacent cores, which is temperature and magnetic field dependent. Hence, E_m is also expected to be temperature and magnetic field dependent, which is essential for the explanation of the experimental results.

Now we turn to discuss the magnetic memory effect (Fig. 3), the two linear HFMC regions (Fig. 4) and the origin of the resistance peak T_p, as well as its sample thickness and magnetic field dependence (Fig. 6).

A. Strong magnetic memory effect of NRN-LCMO shown in Fig. 3

It is related to the spin glass in the shell layer. The shell layer is spin glass disordered at 10 K and thus quite difficult to be aligned by the applied magnetic field. However, the applied magnetic field induces some magnetic alignment anyway and possible change of the electronic state because of the strong coupling between spin and charge degrees of freedoms in manganites, leading to a reduction in tunneling barrier E_m and thus a big decrease in R_b. From Fig. 3, R_b of 36-nm sample decrease quickly as the field is increased. As a result, $\mathrm{MR}=[R(0)-R(H)]/R(0)$ reaches 98% at 4 T for 36 nm sample. Its MC (Fig. 4) has a steady increase without signs of saturation up to 14 T, consistent with the spin glass disordering in the shell. After the magnetic field was withdrawn, spin glass in the shell has a tendency to keep the induced Mn spin alignment.[37] So the NRN-LCMO remains in the low resistance state at low temperatures after the withdrawal of the magnetic field, showing a magnetic field memory effect. As shown by their SEM images in the inset of Fig. 1, the grain of 36-nm sample is much smaller than that of 180-nm sample. Consequently, the thickness of the magnetically disordered shell layer, i.e., the magnetic tunneling barrier width, for the 36-nm sample is much thicker than that of 180-nm sample. That is why the MC of the 36-nm sample is much more pronounced than that of the 180-nm sample and the resultant memory effect is much stronger for 36-nm NRN-LCMO.

B. Two linear HFMC regions shown in Fig. 4

Two linear HFMC regions shown in Fig. 4 may come from the two types of spin glass in the shell layer with different T_g values. For the conventional spin glass, linear and nonlinear magnetization responses to the applied magnetic field (M-H curve) exist, with the linear regime corresponding to higher H.[38] Hence the susceptibility χ of spin glass is not always a constant for all H. The start point for the occurrence of the linear M-H responses (constant χ) changes with dif-

ferent spin glass. It is likely that *M-H* responses in our NRN LCMO samples are similar to the conventional spin glass in this regard. The existence of the two types of spin glass is responsible for the observed abnormal behavior of HFMC. Since the HFMC is proportional to the susceptibility of the grain boundary and the external magnetic field predicted by the inelastic tunneling model,[3,8] the superposition of the two type spin glass contribution could account for the two-slope behavior of HFMC shown in Fig. 4.

C. Origin of the resistance drop at T_p and its sample thickness and magnetic field dependence shown in Fig. 6

Three factors should be considered, i.e., the internal magnetic field coming from the FM core (Fig. 8), the magnetic fluctuations and thermal excitation due to k_BT energy, and the external magnetic field. These three factors affect the spin alignment in the shells and thus determine the resistance of the sample as seen from Eqs. (2) and (4). The internal magnetic field tends to align the spins in the shells. With decreasing temperature, the magnetic fluctuations will be suppressed in both core and shell. As a result, the internal magnetic field increases and the spin alignment in the shell layers is improved. Meanwhile, the suppression of magnetic fluctuations in the shell layers is also helpful to improve the spin alignment in the shell layers. Based on Eq. (4), E_m will decrease with decreasing temperature, leading to a decrease of resistance.

Above T_c, the resistance of the sample increases with decreasing temperature as in the bulk samples. Below T_c, the insulator-metal transition and FM occur only in the cores of the grains. Because R_b has "$\exp[(E_c+E_m)/2k_BT]$" dependence, it is easy to understand the continuous increase of resistance with further temperature decrease. However, E_m reduces with decreasing temperature. So there is a competition between the reduction of E_m with temperature and the temperature dependence of "$\exp[(E_c+E_m)/2k_BT]$." The resistance drop is expected to occur below a critical temperature (T_p) when the reduction of E_m becomes dominant with decreasing temperature. Our experimental results indicate that T_p does exist. So the resistance drop at T_p does not originate from the insulator-metal transition. Coulomb blockade is responsible for the resistance upturn below 50 K. The thickness of the shell layer decreases as the sample thickness is increased and the contact region between grains also increases with increasing grain size.[20] Consequently, the probability for an easy-conducting path will increase with increasing film thickness and the resistance drop is likely to occur at higher temperatures for the thicker samples. That can account for the sample thickness dependence of T_p observed in NRN-LCMO samples.

For the effect of the external magnetic field H on T_p with different film thickness. The contribution of H to the spin alignment in the shell layer comes from two aspects. One is the suppression of the magnetic fluctuations in the FM cores and the alignment of the two adjacent FM cores, which are helpful to the spin alignment in the shells. The other one comes from the direct enhancement of the spin alignment in the shells as H is applied. Both of them make the T_p shift to higher temperatures with increasing H. However, with the increase of T_p, the magnetic fluctuations are also enhanced due to the larger k_BT energy, so the contribution of H to the spin alignment of the shells is attenuated. As a result, the shift amount of T_p coming from each T of the external magnetic field reduces with increasing external magnetic field, which is consistent with the T_p-H plots of the 108-nm and 162-nm samples shown in Fig. 7. Because T_p increases with increasing film thickness, the contribution of H to the shift of T_p will deteriorate with increasing film thickness. When T_p reaches a quite high value through increasing film thickness, the shift amount of T_p induced by H might be unobservable unless the applied magnetic field is very strong. In other words, the T_p of the thicker film might become insensitive to the magnetic field. This is in agreement with the results of the NRN-LCMO with a 200-nm thickness, as shown in Figs. 6 and 7.

The above analysis suggests that the origin of the resistance drop at T_p in NRN-LCMO is different from that of the bulk sample, i.e., the electrical resistance peak here is not due to an insulator-metal transition. This scenario may be also applicable to other cases where T_p and T_c of the manganites are not consistent and the resistance is high, such as the results of Chen *et al.* on the mixed aligned $La_{1-x}MnO_3$ (T_p=195 K),[10] where T_p of the sample does not increase when 5 T external magnetic field is applied. Zhang *et al.*[23] studied the grain size dependence of the transport property in $La_{0.85}Sr_{0.15}MnO_3$ and found a resistivity peak well below T_c. They also argued that the peak is not due to a metal-insulator transition and is instead related to the interfacial tunneling as supported by the theoretical calculation.

Lastly, the reduced connection between nanograins in NRN-LCMO should be mentioned. In nano-CMR materials, the size distribution of nanograins results in a distribution of shell thickness and a subsequent distribution of the potential barriers, which is indicated by our relaxation data discussed above. For the nano-CMR manganites with ultrafine grains obtained by other approaches, the connection of the nanograins is three dimensional and the shell layers constitute three-dimensional conduction path networks leading to a variety of alternative conduction paths in parallel between the two electrodes. However, the conduction path network in our NRN-LCMO is constrained in one or two dimensions, especially for the 36-nm NRN sample whose conduction path may reduced to one path (see its SEM image in Fig. 1). Therefore, there is very little opportunity to choose the least intergrain tunneling barrier E_m channel for the NRN-LCMO due to its constrained geometry. This grain connection difference between NRN-LCMO and nano-CMR manganites with ultrafine grains obtained by other approaches can account for the giant MC in the NRN-LCMO [see Fig. 4(a), 36-nm film] because the effect of magnetic field on resistance is more dramatic for samples with larger tunneling barrier E_m.

IV. SUMMARY

We studied the magnetic and magnetotransport property of NRN-LCMO. The resistance relaxation at zero magnetic field and the exchange bias effect of magnetization were ob-

served, indicating two types of spin glass in the grain shell. This NRN-LCMO shows a giant magnetoconductance and two linear HFMC regions. The resistance peak of NRN-LCMO shifts to high temperatures with magnetic field and becomes insensitive to magnetic field for thicker samples. Based on the multistep inelastic tunneling mechanism and the core-shell model, an unified picture is proposed to account for the origin of the resistance peak, grain size dependence of T_p, insensitivity of T_p to the magnetic field for thicker samples, the memory effect, and the two linear HFMC behaviors. This work indicates that the magnetization state of the shell layer of the LCMO nanograins plays an important role in determining the electronic transport property. NRN-LCMO also provides a way to increase the MC of the nano-CMR manganites.

ACKNOWLEDGMENTS

This work was supported by the National Science Foundation of China (Grant Nos. 50425205, 10674079, 50628202, and 50272031), 973 Project No. 2002CB613505, the Excellent Young Teacher Program of MOE, Specialized Research for the Doctoral Program of Higher Education (Grant No. 20030003088) and the National Center for Nanoscience and Technology of China. We are also grateful to T. Venkatesan, S. Ogale, X. X. Xi, Q. Li, and D. S. Dai for enlightening discussions.

*Email address: ygzhao@tsinghua.edu.cn

[1] H. Y. Hwang, S. W. Cheong, N. P. Ong, and B. Batlogg, Phys. Rev. Lett. **77**, 2041 (1996).
[2] M. Wagenknecht, H. Eitel, T. Nachtrab, J. B. Philipp, R. Gross, R. Kleiner, and D. Koelle, Phys. Rev. Lett. **96**, 047203 (2006).
[3] M. Ziese, A. Bollero, I. Panagiotopoulos, and N. Moutis, Phys. Rev. B **72**, 024453 (2005).
[4] N. Kozlova, K. Dorr, D. Eckert, T. Walter, and K.-H. Muller, J. Magn. Magn. Mater. **261**, 48 (2003).
[5] M. Paranjape, J. Mitra, A. K. Raychaudhuri, N. K. Todd, N. D. Mathur, and M. G. Blamire, Phys. Rev. B **68**, 144409 (2003).
[6] R. Gross, L. Alff, B. Buchner, B. H. Freitag, C. Hofener, J. Klein, Yafeng Lu, W. Mader, J. B. Philipp, M. S. R. Rao, P. Reutler, S. Ritter, S. Thienhaus, S. Uhlenbruck, and B. Wiedenhorst, J. Magn. Magn. Mater. **211**, 150 (2000).
[7] Yeong-Ah Soh, G. Aeppli, N. D. Mathur, and M. G. Blamire, Phys. Rev. B **63**, 020402(R) (2000).
[8] S. Lee, H. Y. Hwang, B. I. Shraiman, W. D. Ratcliff II, and S-W. Cheong, Phys. Rev. Lett. **82**, 4508 (1999).
[9] M. Ziese, Phys. Rev. B **60**, R738 (1999).
[10] C. C. Chen and Alex de Lozanne, Appl. Phys. Lett. **73**, 3950 (1998).
[11] X. L. Wang, S. X. Dou, H. K. Liu, M. Lonescu, and B. Zeimetz, Appl. Phys. Lett. **73**, 396 (1998).
[12] A. Gupta, G. Q. Gong, G. Xiao, P. R. Duncombe, P. Lecoeur, P. Trouilloud, Y. Y. Wang, V. P. Dravid, and J. Z. Sun, Phys. Rev. B **54**, R15629 (1996).
[13] P. Dey and T. K. Nath, Appl. Phys. Lett. **87**, 162501 (2005).
[14] X. S. Wu, W. Cai, X. P. Zhang, Y. G. Zhao and L. Lu, J. Phys.: Condens. Matter **17**, 6981 (2005).
[15] Y. G. Zhao, W. Cai, X. S. Wu, X. P. Zhang, K. Wang, S. N. Gao, L. Lu, and J. Zhu, Appl. Phys. A: Mater. Sci. Process. **81**, 607 (2005).
[16] M. M. Savosta, V. N. Krivoruchko, I. A. Danielenko, V. Yu. Tarenkov, T. E. Konstantinova, A. V. Borodin, and V. N. Varyukhin, Phys. Rev. B **69**, 024413 (2004).
[17] Z. G. Huang, Z. G. Chen, K. Peng, D. H. Wang, F. M. Zhang, W. Y. Zhang, and Y. W. Du, Phys. Rev. B **69**, 094420 (2004).
[18] D. Niebieskikwiat, R. D. Sanchez, D. G. Lamas, A. Caneiro, L. E. Hueso, and J. Rivas, J. Appl. Phys. **93**, 6305 (2003).
[19] T. Zhu, B. G. Shen, J. R. Sun, H. W. Zhao, and W. S. Zhan, Appl. Phys. Lett. **78**, 3863 (2001).
[20] Ll Balcells, J. Fontcuberta, B. Martinez, and X. Obradors, Phys. Rev. B **58**, R14697 (1998); Ll Balcells, B. Martinez, F. Sandiumenge, and J. Fontcuberta, J. Magn. Magn. Mater. **211**, 193 (2000).
[21] J. Rivas, L. E. Hueso, A. Fondado, F. Rivadulla, and M. A. Lopez-Quintela, J. Magn. Magn. Mater. **221**, 57 (2000).
[22] A. de Andres, M. Garcia-Hernadez, J. L. Martinez, and C. Prieto, Appl. Phys. Lett. **74**, 3884 (1999).
[23] N. Zhang, W. P. Ding, W. Zhong, D. Y. Xing, and Y. W. Du, Phys. Rev. B **56**, 8138 (1997).
[24] R. Mahesh, R. Mahendira, A. K. Raychaudhuri, and C. N. R. Rao, Appl. Phys. Lett. **68**, 2291 (1996).
[25] D. G. Lamas, A. Caneiro, D. Niebieskikwiat, R. D. Sanchez, D. Garcia, and B. Alascio, J. Magn. Magn. Mater. **241**, 207 (2002).
[26] M. Muroi, R. Street, and P. G. McCormick, J. Appl. Phys. **87**, 3424 (2000); M. Muroi, R. Street, and P. G. McCormick, *ibid.* **87**, 5579 (2000).
[27] R. H. Kodama, A. E. Berkowitz, E. J. McNiff, Jr., and S. Foner, Phys. Rev. Lett. **77**, 394 (1996).
[28] B. Martínez, X. Obradors, Ll. Balcells, A. Rouanet, and C. Monty, Phys. Rev. Lett. **80**, 181 (1998).
[29] L. D. Bianco, D. Fiorani, A. M. Testa, E. Bonetti, and L. Signorini, Phys. Rev. B **70**, 052401 (2004).
[30] M. Gruyters, Phys. Rev. Lett. **95**, 077204 (2005).
[31] M. Matsukawa, M. Chiba, K. Akasaka, R. Suryanarayanan, M. Apostu, A. Revcolevschi, S. Nimori, and N. Kobayashi, Phys. Rev. B **70**, 132402 (2004).
[32] M. Matsukawa, K. Akasaka, H. Noto, R. Suryanarayanan, S. Nimori, M. Apostu, A. Revcolevschi, and N. Kobayashi, Phys. Rev. B **72**, 064412 (2005).
[33] J. G. Simmons, J. Appl. Phys. **34**, 1793 (1963).
[34] L. I. Glazman and K. A. Matveev, Sov. Phys. JETP **67**, 1276 (1988).
[35] J. S. Helman and B. Abeles, Phys. Rev. Lett. **37**, 1429 (1976).
[36] J. M. D. Coey, A. E. Berkowitz, LI. Balcells, F. F. Putris, and A. Barry, Phys. Rev. Lett. **80**, 3815 (1998).
[37] K. Jonason, E. Vincent, J. Hammann, J. P. Bouchaud, and P. Nordblad, Phys. Rev. Lett. **81**, 3243 (1998).
[38] J. A. Mydosh, *Spin Glasses: An Experimental Introduction* (Taylor & Francis, New York, 1993).